ISSN 0016-7932, Geomagnetism and Aeronomy, 2018, Vol. 58, No. 7, pp. 1008–1013. © Pleiades Publishing, Ltd., 2018.

Compton Scattering of the Hard X-Ray Flux of Solar Flares with Various Angular Anisotropies of Hard X-Ray Sources

E. P. Ovchinnikova[a], *, Yu. E. Charikov[a], A. N. Shabalin[a], and G. I. Vasil'ev[a]

[a] *Ioffe Institute, Russian Academy of Sciences, St. Petersburg, 194021 Russia*

**e-mail: elfimovaevgeniya@gmail.com*

Received February 16, 2018; in final form, March 19, 2018

Abstract—The contribution of photons reflected from the solar photosphere to the intensity and the change in the slope of the energy spectrum of solar flare hard X-rays were analyzed as a function of the X-ray anisotropy. The angular and energy distributions of primary hard X-rays and the position of the flare loop on the solar disk were the main parameters in calculations. The contribution of the reflected component to the total flux for an anisotropic source may be as high as 70% at an energy range of 30–40 keV if the source is shifted relative to the solar disk center. The maximum change in the X-ray spectral index is 0.5.

DOI: 10.1134/S0016793218070150

1. INTRODUCTION

During solar flares, measurements of hard X-rays (HXRs) with a high spatial (up to 2 arcseconds), energy, and time resolution were performed (Lin et al., 2002). The photon spectrum at energies $\epsilon > 25$ keV is formed by the bremsstrahlung of accelerated electrons (Brown, 1971). The flux and the energy spectrum of X-rays detected during solar flares are superpositions of "primary" radiation and radiation reflected from the photosphere as a result of Compton scattering. Penetrating the photosphere, HXR photons undergo Compton scattering, which alters their trajectory and energy, and form the albedo flux. It was demonstrated (Bai and Ramaty, 1978) that the albedo produces a sizable contribution to the total flux in the energy range of 10–100 keV with a maximum at 30–40 keV. Photons with energies higher than 100 keV penetrate deeper into the photosphere, lose their energy, and are absorbed; photons with energies below 10 keV photoelectrically absorbed by their first scattering. The contribution of reflected photons to the observed flux depends not only on their energy but also on the position of the primary source (flare) on the solar disk. The method to determine the albedo contribution for an arbitrary HXR energy distribution was discussed (Kontar et al., 2006), and the dependence of the size of a HXR source on its position of the solar disk was examined (Kontar and Jeffrey, 2010). However, the energy and angular distributions of primary HXR photons are not arbitrary and depend on the parameters of flare plasma and the beam of accelerated electrons.

The goal of the present study is to determine the effect of HXR anisotropy on the reflected and the observed (total) HXR fluxes and to reveal variations in the intensity and the index of the observed HXR spectrum corresponding to different anisotropy models. The angular and energy distributions of primary hard X-rays were calculated in the kinetic model. The distribution function of accelerated electrons at the moment of injection and the distribution of the plasma density and the magnetic field along the flare loop (Hamilton, 1990; Gorbikov and Melnikov, 2007; Charikov and Shabalin, 2016) were the initial parameters. The GEANT4 (GEometry ANd Tracking) toolkit was used to calculate the flux, the energy spectrum, and the angular distribution of scattered photons.

2. PHYSICAL KINETICS OF A BEAM OF ACCELERATED ELECTRONS

The nonstationary relativistic Fokker–Planck equation for accelerated electrons in a magnetic loop can be written in the following form (Charikov and Shabalin, 2016):

$$\frac{\partial f}{\partial t} = -c\beta\mu\frac{\partial f}{\partial s} + c\beta\frac{\partial \ln(B)}{\partial s}\frac{\partial}{\partial \mu}\left[\frac{(1-\mu^2)}{2}f\right] + C_1\frac{c}{\lambda_0}\frac{\partial}{\partial E}\left(\frac{f}{\beta}\right) + C_2\frac{c}{\lambda_0\beta^3\gamma^2}\frac{\partial}{\partial \mu}\left[(1-\mu^2)\frac{\partial f}{\partial \mu}\right] + S(E,\mu,s,t), \quad (1)$$

$$C_1 = x + \frac{1-x}{2}\frac{\ln\beta^2 g^2 E/\alpha_F^4}{\ln\Lambda}, \quad C_2 = \frac{1}{2} + \frac{1+g}{4}C_1,$$

$$\lambda_0(s) = 10^{24}/n(s)\ln\Lambda\ , \ \beta = \frac{v}{c},$$

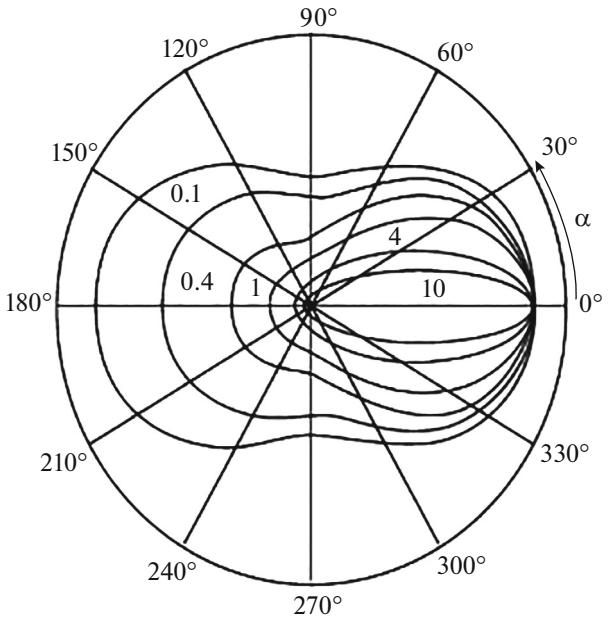

Fig. 1. Diagram of the spatial distribution of the differential cross section of Compton scattering for various photon energies E_{ph}/mc^2 (indicated next to curves); α is the photon scattering angle with respect to the direction of motion of a primary photon (Fetisov, 2017).

$\mu = \cos(\varphi)$, φ is the pitch angle of an electron, $\gamma = E + 1$ is the Lorentz factor, and E is the kinetic energy of an electron (in units of the electron rest energy).

The transfer of electrons along a magnetic loop, magnetic reflection in a convergent magnetic field, collisional energy losses, and Coulomb scattering in plasma are taken into account in (1). The last term in Eq. (1) characterizes the electron distribution function at the moment of injection. The considered problem is spatially one-dimensional. The function of the electron source is presented in factorized form (independent distributions over energy, angle, space, and time):

$$S(E,\varphi,s,t) = S_1(E)S_2(\varphi)S_3(s)S_4(t). \qquad (2)$$

The energy spectrum of electrons is a power-law one:

$$S_1(E) = K\left(\frac{E}{E_0}\right)^{-\nu},$$

$$S_2(\varphi) = \cos^{12}\varphi.$$

The time and coordinate distribution function has a Gaussian form:

$$S_3(s) = \exp\left(-\frac{(s-s_1)^2}{s_0^2}\right),$$

$$s_0 = 2\times10^8 \text{ cm}, \quad s_1 = 0 \text{ cm},$$

$$S_4(t) = \exp\left(-\frac{(t-t_1)^2}{t_0^2}\right), \quad t_1 = 2.6 \text{ s}, \quad t_0 = 1.4 \text{ s}.$$

Using the method of total approximation for multidimensional problems, we calculate numerically the distribution function of accelerated electrons. The intensity of X-ray radiation of accelerated electrons is calculated by the formulas for relativistic bremsstrahlung (Bai and Ramaty, 1978).

3. SIMULATION OF COMPTON SCATTERING

The GEANT4 toolkit (Allison, 2016), which utilizes the Monte Carlo method, was used to model the processes of interaction (photoeffect, Compton scattering) of photons in their propagation through the photosphere. The number of primary photons emitted by a single source exceeded 10^8. Using the process cross-sections for a given photon energy, we simulated the scattering angles and energies for each quantum. As the photon energy increases, the reflected X-ray radiation becomes more directed (Fig. 1), and the probability of scattering in the opposite direction decreases. The probability of photoeffect increases as the photon energy decreases as a result of Compton scattering. The possibility of multiple Compton scattering was taken into account, since multiple scattering becomes more probable (due to an increase in the thickness of the medium traversed by a photon) at small angles between the photon trajectory and the normal to the solar surface. The photosphere, the chromosphere, and deeper layers were represented by 54 concentric spherical layers with a constant density ranging from 1.9×10^{-12} to 5.2×10^{-6} g cm^{-3}. The energy of primary photons was higher than 25 keV, since the contribution of thermal plasma electrons to hard X-rays is almost nonexistent at such energies.

4. CALCULATION OF THE BACKSCATTERED RADIATION FLUXES AT VARIOUS ANISOTROPIES OF PRIMARY HARD X-RAY

The angular anisotropy of the primary HXR source is an important factor in calculations of the contribution of the reflected photon flux. In the present study, the anisotropic photon model is analysed with calculated angular distribution in the kinetic model of an accelerated electron beam. Figure 2 presents the anisotropic angular distribution of primary HXR photons. The ratio of the flux of photons emitted in the direction away from the Sun and unscattered ("primary" radiation) to the total flux is $\frac{Q_{\text{primary}}}{Q_{\text{total}}} = 18\%$ for this angular distribution. The scattered X-ray flux depends on the relative position of the observer and the HXR source (i.e., on the source position on the solar disk). We shifted the source position from the disk center to the limb (the heliocentric angle varied from 0° to 90°). Figure 3 shows the reflected, primary, and total photon fluxes for the anisotropic model with

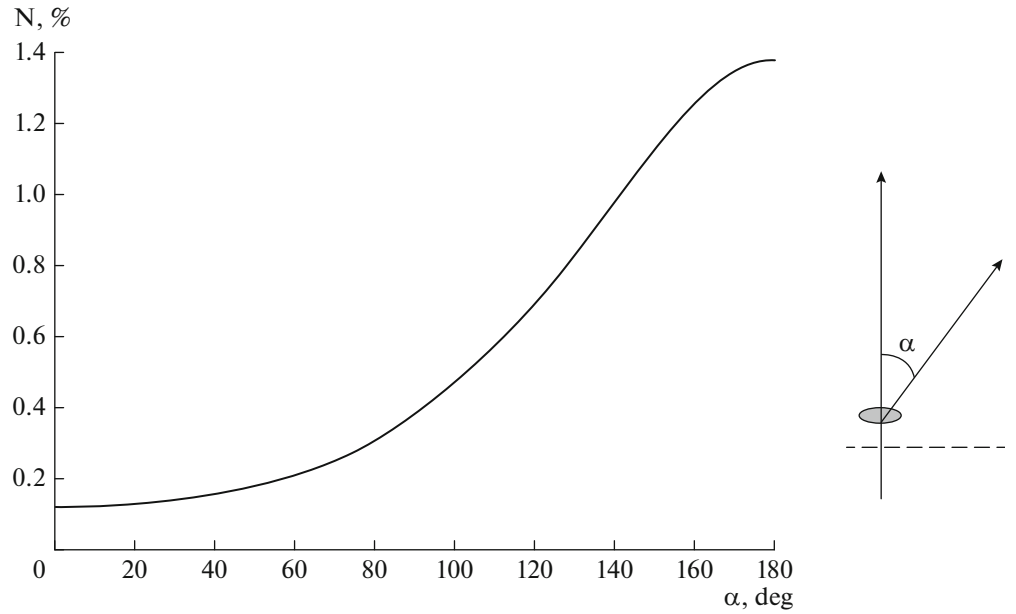

Fig. 2. Left: energy-averaged angular distribution of HXR photons obtained in the kinetic model; α is the angle between the normal to the photosphere surface at the given point and the photon trajectory. Right: illustration clarifying the choice of α.

a power-law energy dependence $I(\epsilon) = \epsilon^{-\gamma}$, where $\gamma = 3$ and the heliocentric angle is $\theta = 0°$. The backscattered component dominates in the observed total flux up to 100 keV and thus alters the slope of the primary spectrum. In order to assess the spectrum change due to source anisotropy, we excluded other factors (such as the relation between angular and energy characteristics) by setting the same energy dependence at different angular distributions. The power-law HXR photon spectrum $I(\epsilon) = \epsilon^{-\gamma}$ with $\gamma = 3$ and 5 was used, and the spectra of observed, reflected, and primary X-rays were determined.

Figure 4 presents the ratios of the backscattered photon flux to the total flux for isotropic and anisotropic models. The contribution of reflected photons to the total flux for isotropic sources increases as the flare location shifts from the limb to the center of the solar disk; its maximum is 40% at 30–40 keV. This agrees with the results reported by Kontar et al. (2006). The maximum contribution for anisotropic models (70% at 30–40 keV) may be observed with the source shifted away from the disk center. The maximum for the models under consideration is observed at a heliocentric angle of 40° (Fig. 4).

In order to examine the change in the HXR spectrum slope, the obtained fluxes were approximated with a broken power law with an break point at 40–50 keV. Figure 5 shows the dependence of the index on the flare position on the solar disk in two energy intervals. The spectrum slope changes slightly in the 30–40 keV region, where the contribution of reflected photons to the flux reaches its maximum. The maximum change in the HXR spectral index is $\gamma \sim 0.5$ in the 50–200 keV region. The slope variation becomes less significant as the source shifts from the disk center to the limb.

It is not possible to characterize accurately the energy distribution of photons obtained in the kinetic model by a power law or to relate it to the angular distribution of photons. The change in the spectrum slope for this model may be characterized by parameter δ written as

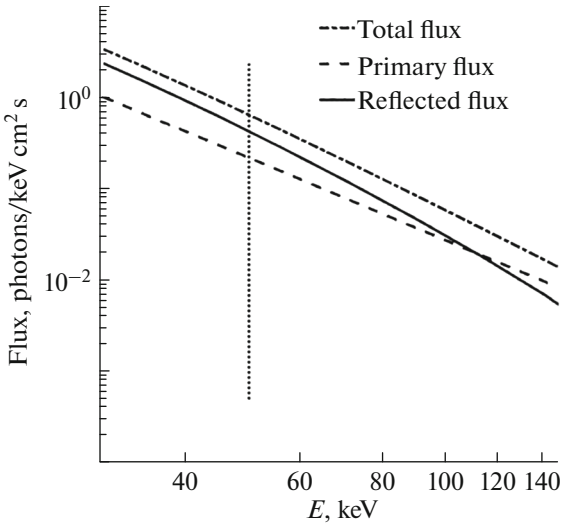

Fig. 3. Primary, backscattered, and total HXR fluxes for the anisotropic model with a power-law energy spectrum with index $\gamma = 3$ and the source located at the center of the solar disk.

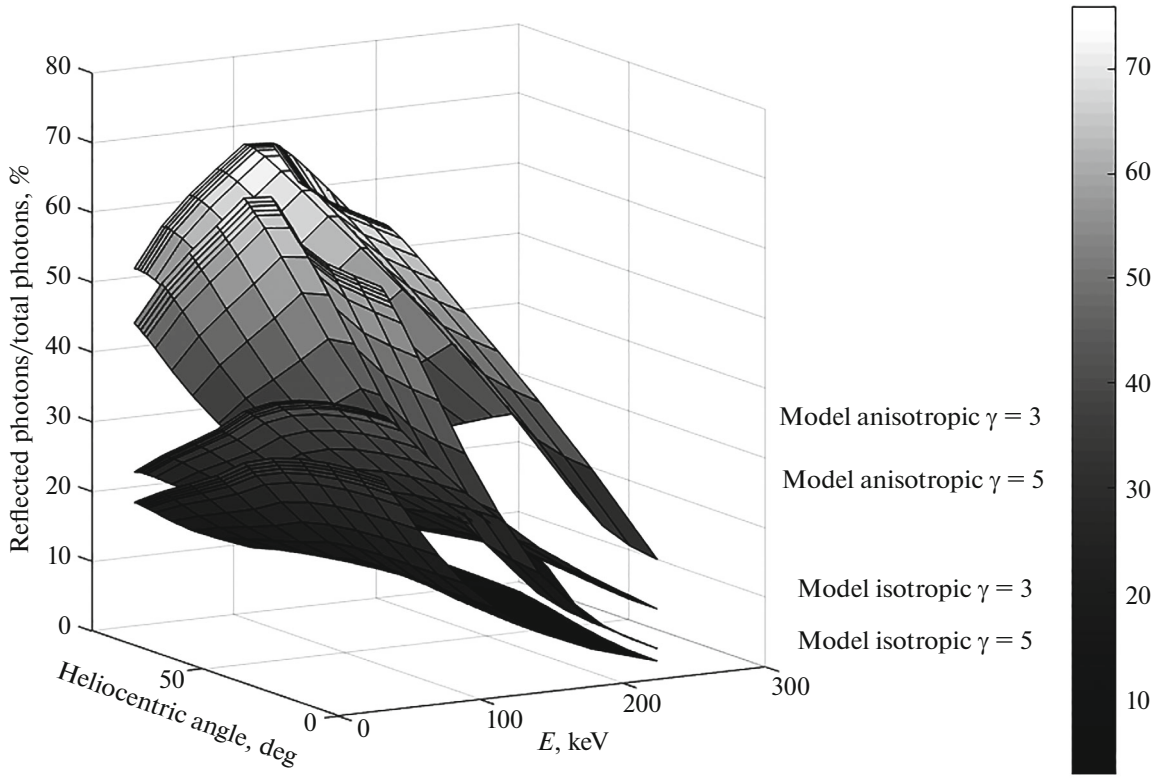

Fig. 4. Contribution of backscattered photons to the total HXR flux for various models of the electron beam and plasma.

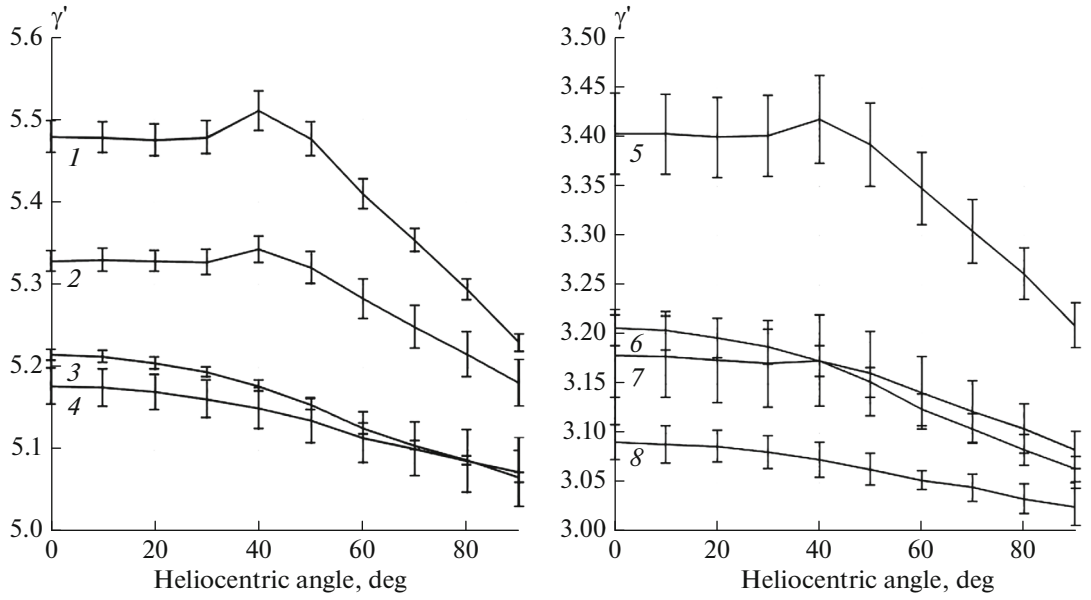

Fig. 5. Variation of index γ' of the observed HXR spectrum (approximation with a power law in the given energy interval) with the source position on the solar disk. The curves correspond to the following models (the energy distribution of primary photons was set in the form of a power law with index γ): (*1*) anisotropic model (γ = 5 in the 50–200 keV interval); (*2*) anisotropic model (γ = 5 in the 30–40 keV interval); (*3*) isotropic model (γ = 5 in the 50–200 keV interval); (*4*) isotropic model (γ = 5 in the 30–40 keV interval); (*5*) anisotropic model (γ = 3 in the 50–200 keV interval); (*6*) isotropic model (γ = 3 in the 50–200 keV interval); (*7*) anisotropic model (γ = 3 in the 30–40 keV interval); (*8*) isotropic model (γ = 3 in the 30–40 keV interval).

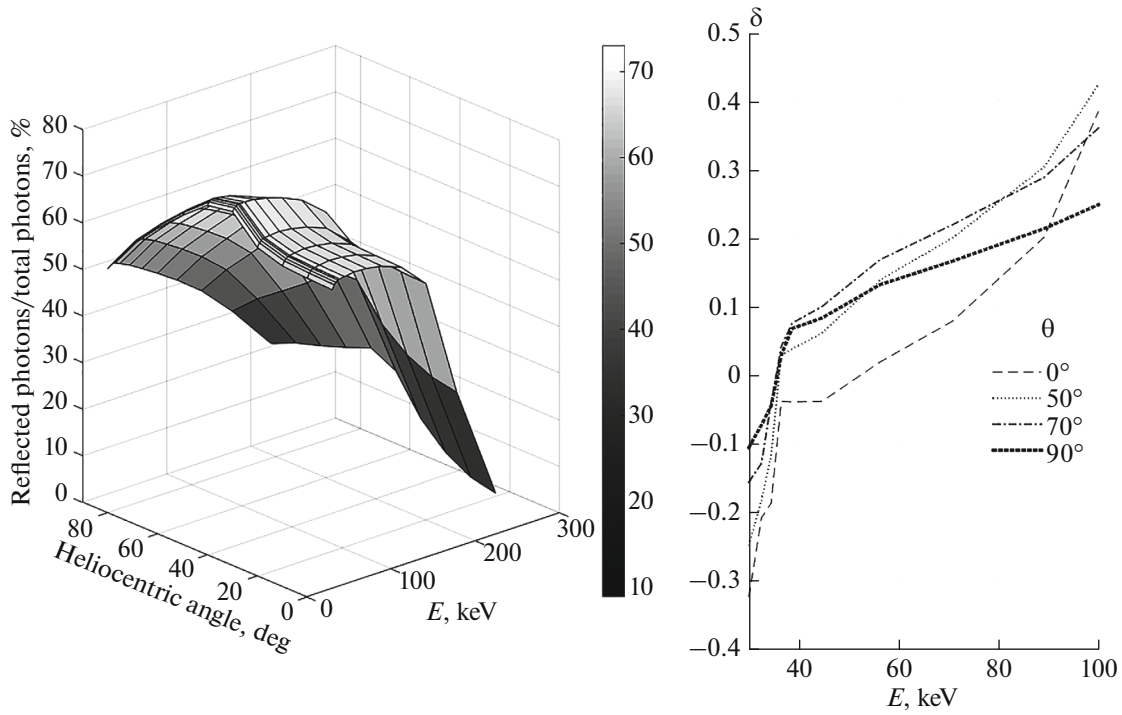

Fig. 6. Left: contribution of reflected photons to the total flux. Right: variation δ of the spectrum slope upon the introduction of Compton scattering for the model with interrelated energy and angular dependences.

$$\delta = \gamma' - \gamma,\ \ \gamma' = \frac{-d\ln I'(\epsilon)}{d\ln\epsilon},\ \ \gamma = \frac{-d\ln I(\epsilon)}{d\ln\epsilon}. \qquad (3)$$

Here, I and I' are the intensities of primary and total hard X-rays, and ϵ is the photon energy.

Parameter $\delta < 0$ at 30–50 keV, which corresponds to spectrum hardening in this interval. At energies higher than 50 keV, $\delta > 0$ (the spectrum softening; see Fig. 6). The highest ratio of the reflected flux to the total flux is 70% (Fig. 6); this maximum for the anisotropic model is observed at a heliocentric angle of 40^0.

5. CONCLUSIONS

Primary and back-scattered X-rays of solar flares were calculated. The HXR spectrum changes induced by Compton scattering were examined. In the case of an anisotropic source of accelerated electrons, the contribution of the reflected component to the total flux may exceed that of the primary flux at energies up to 100 keV, and the ratio of backscattered photons to overall number at 30–40 keV may be as high as 70%. It is also important to take into account the flare position on the disk. The contribution of the Compton component to the total flux may be maximized in the case of an off-center flare loop and an anisotropic flux of primary quanta. For example, the maximum intensity for the considered models was observed at heliocentric angle $\theta = 40°$. The spectrum slope for these models varies insignificantly under the influence of albedo; the maximum change was 0.5. The HXR measurements performed during solar flares by modern observatories (e.g., RHESSI) reveal changes in the spectrum slope that are as small as 0.1–0.3. The maximum change in the spectrum slope is found in the regions with the smallest contribution of reflected photons to the observed flux. For example, the maximum variation was observed in the 50–100 keV region, while the Compton scattering is more efficient at lower particle energies. If the models with interrelated energy and angular dependences are considered, the HXR spectrum differs from a power-law one. Parameter δ, which characterizes the slope change within each energy interval, should be used in this case to analyze such slope variations. At 30–50 keV, $\delta < 0$ (i.e., the spectrum gets harder in this region). At energies higher than 50 keV, the albedo makes the spectrum softer. In general the albedo effect leads to softening of the observed HXR spectrum.

ACKNOWLEDGMENTS

The work of E.P. Ovchinnikova, Yu.E. Charikov, and A.N. Shabalin was supported by the Russian Science Foundation, grant no. 17-12-01378.

REFERENCES

Allison, J., Amako, K., Apostolakis, J., Arce, P., and Asai, M., Recent developments in Geant4, *Nucl. Instrum. Methods Phys. Res., Sect. A*, 2016, vol. 835, pp. 186–225.

Bai, T. and Ramaty, R., Backscatter, anisotropy, and polarization of solar hard X-rays, *Astrophys. J.*, 1978, vol. 219, pp. 705–726.

Brown, J.C., The deduction of energy spectre of non-thermal electrons in flares from the observed dynamics spectra of hard X-ray burst, *Sol. Phys.*, 1971, vol. 18, pp. 489–502.

Charikov, Y.E. and Shabalin, A.N., Hard X-ray generation in the turbulent plasma of solar flares, *Geomagn. Aeron. (Engl. Transl.)*, 2016, vol. 56, no. 8, pp. 1068–1074.

Fetisov, G., *Sinkhrotronnoe izluchenie. Metody issledovaniya struktury veshchestv* (Synchronous Radiation. Methods for Studying the Structure of Matter), Moscow: Fizmatlit, 2007.

Gorbikov, S.P. and Melnikov, V.F., The numerical solution of the Fokker–Planck equation for modeling of particle distribution in solar magnetic traps, *Mat. Model.*, 2007, vol. 19, no. 2, pp. 112–122.

Hamilton, R.J., Lu, E.T., and Petrosian, V., Numerical solution of the time-dependent kinetic equation for electrons in magnetized plasma, *Astrophys. J.*, 1990, vol. 354, pp. 726–734.

Kontar, E.P. and Jeffrey, N.L.S., Positions and sizes of C-ray solar flare sources, *Astron. Astrophys.*, 2010, vol. 513, p. L2.

Kontar, E.P., MacKinnon, A.L., Schwartz, R.A., and Brown, J.C., Compton backscattered and primary X-rays from solar flares: Angle dependent Green's function correction for photospheric albedo, *Astron. Astrophys.*, 2006, vol. 446, no. 3, pp. 1157–1163.

Krucker, S., Battaglia, M., Cargill, P.J., Fletcher, L., and Hudson, H.S., Hard X-ray emission from the solar corona, *Astron. Astrophys. Rev.*, 2008, vol. 16, nos. 3–4, pp. 155–208.

Lin, R.P., Dennis, B.R., and Hurford, G.J., The Reuven Ramaty high-energy solar spectroscopic imager (RHESSI), *Sol. Phys.*, 2002, vol. 210, no. 5, pp. 3–32.

Translated by D. Safin